ELSEVIER

Physica A 297 (2001) 37–63

PHYSICA A

www.elsevier.com/locate/physa

Interior Stokes flows with stick-slip boundary conditions

D. Palaniappan, Prabir Daripa*

Department of Mathematics, Texas A&M University, College Station, Texas-77843-3368, USA

Received 23 January 2001

Abstract

Two-dimensional Stokes flows generated by line singularities inside a circular cylinder are studied in the presence of stick-slip boundary conditions. For simplicity, line singularities are assumed to be parallel to the cylinder axis, all axes in the same plane. The interior boundary value problem associated with these flows is solved in terms of a stream function. Analytic solutions are obtained for flows induced by a rotlet, a potential-source and Stokeslets with axes radial (normal) or tangential to the cylinder by the Fourier expansion method. These solutions are used to plot streamline topologies of these flows and the flow patterns are studied as the slip parameter and the locations of the singularities are varied. Eddies of various sizes and shapes appear as the slip parameter is varied.

Interesting flow patterns are observed in flows generated by a pair of rotlets. In this case, streamline patterns reveal interesting flow topologies. Some of the flow patterns observed here are similar to that of vortex mixing flows. Interior saddle points are found in these flows for certain values of the slip parameter and locations of the rotlets. The flows induced by a source and a sink and a pair of Stokeslets also exhibit interesting features. The plots of the fluid velocity on the surface of the cylinder show the locations of surface stagnation points, if they exist. A study of the movement of surface stagnation points as the slip parameter and the locations of the singularities are varied shed some light on the qualitative features of the flow patterns. The results presented may be relevant for a variety of applications including vortex mixing and journal bearing flows.

1. Introduction

Bounded viscous flows are abound in nature as well as in many areas of practical interest such as journal bearing, stirring and mixing of viscous fluids, etc. An insight into various mechanisms and flow topologies of such flows with respect to available free

* Corresponding author.
E-mail address: prabir.daripa@math.tamu.edu (P. Daripa).

0378-4371/01/$ - see front matter
PII: S0378-4371(01)00226-6

parameters can be beneficial to improving the performance of various systems involving such flows. To gain such insight, it is usually desirable to design models that retain the basic flow features of the complex problem, yet simple enough to be analyzed accurately using a combination of analysis and numerics. The most common model used to demonstrate stirring process is the two-dimensional Stokes flows generated by singularities inside a circular cylinder. In these models, a line rotlet, which may be regarded as a rotating cylinder of infinitesimal radius, has been used as a model for a stirrer. Incidentally, this flow is topologically equivalent to the flow between two eccentric circular cylinders with inner or both cylinders rotating which models flow in a journal bearing (see [1] for a comprehensive analysis of journal bearing flows). It is worth citing the work of Jana et al. [2] who have recently attempted to explain vortex mixing flows using two finite cylinders rotating slowly in a cylindrical volume of viscous fluid. There are many studies of mixing and other interior Stokes flows which are not cited here but can be found in the literature. All these studies make use of the no-slip conditions at the boundary of the cylinder.

In this paper, we include stick-slip conditions at the boundary to study interior Stokes flows induced by line singularities of the type that can be used to model various physical effects. These boundary conditions are more general and allow choices of boundary conditions ranging from no-slip to pure-slip. There are many situations where such boundary conditions could be more appropriate. For example, if the boundary were coated with polymer. In the presence of such boundary conditions in the interior of a circular cylinder, we derive exact representation of solutions induced by following types of line singularities: (i) a rotlet, (ii) a potential source, and (iii) Stokeslets with axes tangential or radial (normal) to the cylinder. Using Matlab, we have explored various flow features of these flows which are discussed later in this paper.

We must state right at the outset that novelty of this paper is in the consideration of these stick-slip boundary conditions. To the best of the authors' knowledge, these flows with stick-slip boundary conditions have not been studied to-date. The stick-slip boundary conditions considered here provide the possibilities of a richer and interesting variety of flow patterns as shown in this paper. Some of these interior flows with no-slip boundary condition have been considered before by other investigators. For example, rotlet-induced flows with no-slip boundary conditions have been considered by Ranger [3] and Meleshko et al. [4] independently. These works have shown the existence of attached eddies in some cases. The flow patterns possible in these studies are limited by the fact that the fluid does not slip at the surface. The rotlet flows examined in this paper exhibit some interesting features including existence of saddle points which have been noticed in studies with no-slip boundary conditions. The solution for a source–sink combination located at diagonally opposite boundary points has been obtained by Rayleigh [5] with no-slip boundary conditions. Later we also discuss the solution for a source–sink problem located inside a circular cylinder with stick-slip conditions. Needless to mention that our solution differs from that discussed by Rayleigh [5]. The solutions for Stokeslet problems have not been addressed in the literature even with no-slip conditions.

It is well known that incompressible two-dimensional flows may be viewed as Hamiltonian dynamical systems. In the theory of dynamical systems, interior saddle points (more commonly termed hyperbolic fixed points in the theory) play an important role. A hyperbolic fixed point in steady Hamiltonian system with one degree of freedom is responsible for producing a homoclinic or heteroclinic orbit. A time-periodic perturbation of a steady flow possessing such orbits generally disrupts them causing homoclinic or heteroclinic tangles, a phenomenon indicative of nonintegrable or chaotic dynamics for passively advected particles in the flow (see [7] for an examination of chaos in Hamiltonian systems). This idea has been used in [8–10] to generate chaos in numerical simulation of a time-modulated version of journal bearing flow. Furthermore, it is known that chaotic advection can be used to cause efficient stirring [6]. Consequently, a time-periodic perturbation, e.g. resulting from a periodic motion of the rotlet, of the singularities of some of the flows considered in this paper may exhibit chaos, and therefore enhanced stirring efficiency for cases in which the unperturbed flow possesses a hyperbolic fixed point. Hence, the results given in this article be relevant for the design of efficient stirring devices.

The paper presents a collection of formulae, derived here for the first time, and streamline topologies for various singularity driven two-dimensional Stokes flows inside a cylinder which include the effect of slip. These are assembled in one place here where they might be more accessible for comparison with solutions obtained by numerical computation. The layout of the paper is as follows. The general problem is formulated in terms of stream function in Section 2. The solution for the general problem is derived in Section 3 using Fourier expansion method. The solutions for flows induced by a rotlet, a source, and Stokeslet are given in Section 4. The detailed discussion of the flow features and velocity components in each case is also provided in the respective sections. Finally, the concluding remarks are made in Section 5.

2. Mathematical formulation

We consider two-dimensional steady creeping flows of a viscous incompressible fluid inside an infinitely long circular cylinder of radius a. (The flow considered is essentially two dimensional in a plane perpendicular to the axis of the cylinder). The governing equation for the steady Stokes' flows in terms of stream function ψ is given by

$$\nabla^4\psi = 0\,, \tag{2.1}$$

where ∇^4 is the usual biharmonic operator. The radial and tangential velocity components q_r and q_θ are given by

$$q_r = -\frac{1}{r}\frac{\partial\psi}{\partial\theta}, \quad q_\theta = \frac{\partial\psi}{\partial r}\,, \tag{2.2}$$

where (r,θ) are the polar coordinates.

We seek solutions of Eq. (2.1) for ψ subject to appropriate boundary conditions at the surface of the cylinder. No-slip (stick) boundary condition is often used in

fluid flow problems. A variety of problems has been solved in various contexts using stick boundary conditions. Here, we use the stick-slip conditions at the surface of the cylinder. These conditions contain no-slip and pure-slip (stress-free) conditions as special cases. The stick-slip boundary conditions may be stated as follows.

- Normal velocity is zero at the boundary i.e., $q_r = 0$ at $r = a$;
- Tangential velocity is proportional to the tangential stress at the surface of the cylinder i.e., $q_\theta = (\lambda/\mu)T_{r\theta}$, where

$$T_{r\theta} = \mu\left[\frac{1}{r}\frac{\partial q_r}{\partial\theta} + r\frac{\partial}{\partial r}\frac{q_\theta}{r}\right]$$

is the tangential stress and $\lambda \geqslant 0$ is the slip coefficient.

In terms of stream function ψ, the above conditions become

$$\left.\begin{aligned}&\psi = 0,\\ &\frac{\partial\psi}{\partial r} = \lambda r\frac{\partial}{\partial r}\frac{1}{r}\frac{\partial\psi}{\partial r}\end{aligned}\right\} \quad \text{on } r = a\,. \tag{2.3}$$

The second condition reduces to the usual no-slip condition and the perfect-slip condition for small ($\lambda \to 0$) and large ($\lambda \to \infty$) values of the parameter λ, respectively. It should be pointed out that similar conditions have been used by several authors [11–17] to solve exterior flow problems past a sphere. Next we use these conditions to solve interior flow problems induced by singularities inside a circular cylinder.

In the case of singularity driven flows, in addition to (2.3) we also have the condition

$$\psi \sim \psi_0 \quad \text{as } R_1 \to 0\,, \tag{2.4}$$

where ψ_0 corresponds to the basic flow without the cylinder and R_1 is the distance of the field point measured from the singularity. Below, we present a solution scheme for the general problem discussed above and use it, in later sections, to obtain explicit solutions for a variety of singularity driven flow problems inside a cylinder.

3. Solution scheme

It is convenient and simple to use the Fourier series technique to solve the problem stated in the previous section. The unbounded flow ψ_0 in the absence of the cylinder is expanded as

$$\psi_0(r,\theta) = G(r) + \sum_{n=1}^{\infty}\left[\frac{\alpha_n}{r^n} + \frac{\beta_n}{r^{n-2}}\right] f_n(\theta)\,. \tag{3.1}$$

Here, $f_n(\theta) = a_n\cos n\theta + b_n\sin n\theta$, and α_n, β_n, a_n, b_n are known constants. The function $G(r)$ is a known function of r alone associated with the given flow. The Fourier representation of the complete solution in the interior domain can be taken as

$$\psi(r,\theta) = \psi_0 + A_0 + B_0 r^2 + \sum_{n=1}^{\infty}[A_n r^n + B_n r^{n+2}] f_n(\theta)\,. \tag{3.2}$$

The constants A_0 and B_0 satisfying the boundary conditions will be found later in each singularity driven flow problem with the aid of the function $G(r)$. The unknown Fourier coefficients A_n and B_n for $n \geqslant 1$ may be calculated separately by applying the boundary conditions (2.3). These coefficients are given by

$$a^n A_n = \frac{(n+1)(1-\lambda_1)\alpha_n/a^n + (n\beta_n/a^{n-2})(1-2\lambda_1)}{n\lambda_1 - 1 + \lambda_1}, \tag{3.3}$$

$$a^{n+1} B_n = -\frac{n\alpha_n/a^{n+1} + (n-1)(1-\lambda_1)\beta_n/a^{n-1}}{n\lambda_1 - 1 + \lambda_1}, \tag{3.4}$$

where $\lambda_1 = 2\lambda/(1+2\lambda)$, $0 \leqslant \lambda_1 \leqslant 1$. The corresponding coefficients for a rigid cylinder with stick boundary conditions may be obtained from (3.3) and (3.4) by setting $\lambda_1 = 0$. In this case, the coefficients A_n and B_n become

$$\begin{aligned} a^n A_n &= -\left[(n+1)\frac{\alpha_n}{a^n} + \frac{n\beta_n}{a^{n-2}}\right], \\ a^{n+1} B_n &= \left[\frac{n\alpha_n}{a^{n+1}} + (n-1)\frac{\beta_n}{a^{n-1}}\right]. \end{aligned} \tag{3.5}$$

Another noteworthy special case arises in the limit $\lambda_1 \to 1$. In this case, boundary of the cylinder is impervious and stress free. Taking the limit $\lambda_1 \to 1$ in (3.3) and (3.4), we obtain

$$a^n A_n = -\frac{\beta_n}{a^{n-2}}, \quad a^{n+1} B_n = -\frac{\alpha_n}{a^{n+1}}, \tag{3.6}$$

which are the corresponding results for a cylinder with perfect-slip condition. In the following, we derive solutions for some singularity driven flow problems by using the results derived above.

4. Singularity induced flows inside a cylinder

The simple methodology outlined above may be applied, in principle, to solve a variety of flow problems. Here we use it to obtain exact analytical solutions for several singularity driven flows inside a cylinder. This has been possible because, as will be seen below, we are able to sum the Fourier series in all these cases. These closed form exact solutions for the stream functions are used below to illustrate the effect of slip on the flow patterns and other physical quantities.

For our purposes, the cylinder axis is taken to be parallel to the axes of all primary line singularities, and all these axes lie in a plane containing the cylinder axis. The 2D flow considered is within a disk (cross-section of the cylinder) where all singularities as well as the axis of the cylinder appear as points on the x-axis (i.e., the axis defined by $\theta = 0$ and $-a \leqslant r \leqslant a$) of the coordinate system, with the center of the disk taken as the origin of the coordinate system. Below, we consider various singularity induced flow problems inside this disk.

4.1. Rotlet inside a circular cylinder

The stream function for Stokes flow in an unbounded fluid due a line rotlet of strength F located at $r = c < a$, is given by

$$\psi_0 = F \log R_1 ,$$

where $R_1^2 = r^2 - 2cr\cos\theta + c^2$. The Fourier expansion of ψ_0 for $c < r$ is

$$\psi_0 = F \log r - F\sum_{n=1}^{\infty} \frac{c^n}{nr^n} \cos n\theta . \tag{4.1}$$

Comparison of (4.1) with (3.1) yields

$$G(r) = F \log r, \quad \alpha_n = -\frac{F}{nc^n}, \quad \beta_n = 0 \quad \text{for all } n \geqslant 1 .$$

Now if a circular cylinder is introduced enclosing this rotlet, then the coefficients A_n and B_n, from (3.3) and (3.4), become

$$A_n = \frac{1}{n\lambda_1 - 1 + \lambda_1}\left[(n+1)(1-\lambda_1)\frac{\alpha_n}{a^{2n}}\right] ,$$

$$B_n = -\frac{1}{n\lambda_1 - 1 + \lambda_1}\left[\frac{n\alpha_n}{a^{2n+1}}\right] . \tag{4.2}$$

The constants A_0 and B_0 in the present problem (calculated with the aid of $G(r)$) are given by

$$A_0 = -\log a + \frac{1}{2(1-\lambda_1)}, \qquad B_0 = \frac{1}{2a^2(1-\lambda_1)} .$$

Substitution of the values of these constants in (3.2) yields the required Fourier series solution of the problem. The resulting series can be summed in a straightforward manner to obtain the following exact expression for the stream function:

$$\psi(r,\theta) = F\left[\log R_1 - \log\frac{cR_2}{a} + \frac{1}{2(1-\lambda_1)}\left(1 - \frac{r^2}{a^2}\right) + \left(1 - \frac{r^2}{a^2}\right) r^{(1-\lambda_1)/\lambda_1} I_1\right] , \tag{4.3}$$

where

$$I_1 = \frac{1}{\lambda_1}\int_0^r \rho^{(\lambda_1 - 1)/\lambda_1}\left(\frac{\rho - a^2/c\cos\theta}{R_{1\rho}^2}\right) \mathrm{d}\rho , \tag{4.4}$$

$$R_2^2 = r^2 - \frac{2a^2}{c} r\cos\theta + \frac{a^4}{c^2} , \tag{4.5a}$$

$$R_{1\rho}^2 = \rho^2 - 2c\rho\cos\theta + c^2 . \tag{4.5b}$$

The term involving an integral appears in the solution due to partial slip at the cylinder surface. This integral does not arise in the corresponding solution with stick (no-slip) boundary condition. It can be shown that in the limit $\lambda_1 \to 0$, (4.3) becomes

$$\psi(r,\theta) = F\left[\log R_1 - \log\frac{c}{r}R_2 + \frac{(r^2 - a^2)}{a^2c^2R_2^2}(r^2c^2 - a^4)\right] . \tag{4.6}$$

This agrees with the solution obtained independently by Ranger [3] and Meleshko et al. [4]. We note that in the limit $\lambda_1 \to 1$ corresponding to pure-slip condition, the coefficients A_0 and B_0 become indeterminate. However, if we introduce a term $-F \log r$ along with the given flow ψ_0, then the coefficients A_0 and B_0 become finite in this special case. The term $\log r$ represents a flow due to a rotlet located at the origin. It follows that an off-centered rotlet induced flow does not exist unless there is also a rotlet at the center of the cylinder.

It is of interest to visualize the flow fields by plotting the level sets of stream functions for a single rotlet and a pair of rotlets. For a single rotlet case, the stream function is given by (4.3). For a pair of rotlets, the rotlet locations (r, θ) are taken to be $(c, 0)$ and (c', π) and their strengths F and F', respectively. Needless to say, the complete solution here is obtained by linear superposition principle. For completeness, we give the solution for a rotlet of strength F' located at (c', π) which can be derived in a similar manner. In this case $\psi_0 = F' \log R_1'$, where $R_1'^2 = r^2 + 2cr\cos\theta + c^2$ and the complete solution is given by

$$\psi(r,\theta) = F' \left[\log R_1' - \log \frac{c' R_2'}{a} + \frac{1}{2(1-\lambda_1)} \left(1 - \frac{r^2}{a^2}\right) + \left(1 - \frac{r^2}{a^2}\right) r^{(1-\lambda_1)/\lambda_1} I_1' \right], \tag{4.7}$$

where

$$I_1' = \frac{1}{\lambda_1} \int_0^r \rho^{(\lambda_1 - 1)/\lambda_1} \left(\frac{\rho - a^2/c' \cos\theta}{R_{1\rho}'^2} \right) \mathrm{d}\rho\,, \tag{4.8}$$

$$R_2'^2 = r^2 + \frac{2a^2}{c'} r\cos\theta + \frac{a^4}{c'^2}, \qquad R_{1\rho}'^2 = \rho^2 + 2c'\rho\cos\theta + c'^2\,. \tag{4.9}$$

Below we show some interesting flow patterns induced by a single rotlet and a pair of rotlets for different values of the slip parameter and the primary singularity locations (c, c'). We use the terminology 'a pair of opposite rotlets' to refer to two rotlets of same strengths but of different sign; 'a pair of equal rotlets' to mean two rotlets of same strengths and same sign. Similarly, equidistant rotlets mean a pair of rotlets located equidistant from the center on either side of the x-axis, i.e., $c = c'$.

Similar terminologies for sources and Stokeslets have been used in later subsections.

4.1.1. Single rotlet

The flow structures for various choices of rotlet location and slip parameter λ_1 have been analyzed. Three qualitatively different flow structures emerge: (i) structure composed of circular streamlines extending up to the cylinder; (ii) structure composed of eddies detached from the wall and engulfed within circular streamlines extending up to the cylinder; and (iii) structure composed of eddies which are attached to the wall.

For a rotlet located at the center of the cylinder, flow structure of the first kind appears, as expected, for all admissible values of λ_1. As the rotlet is moved away from

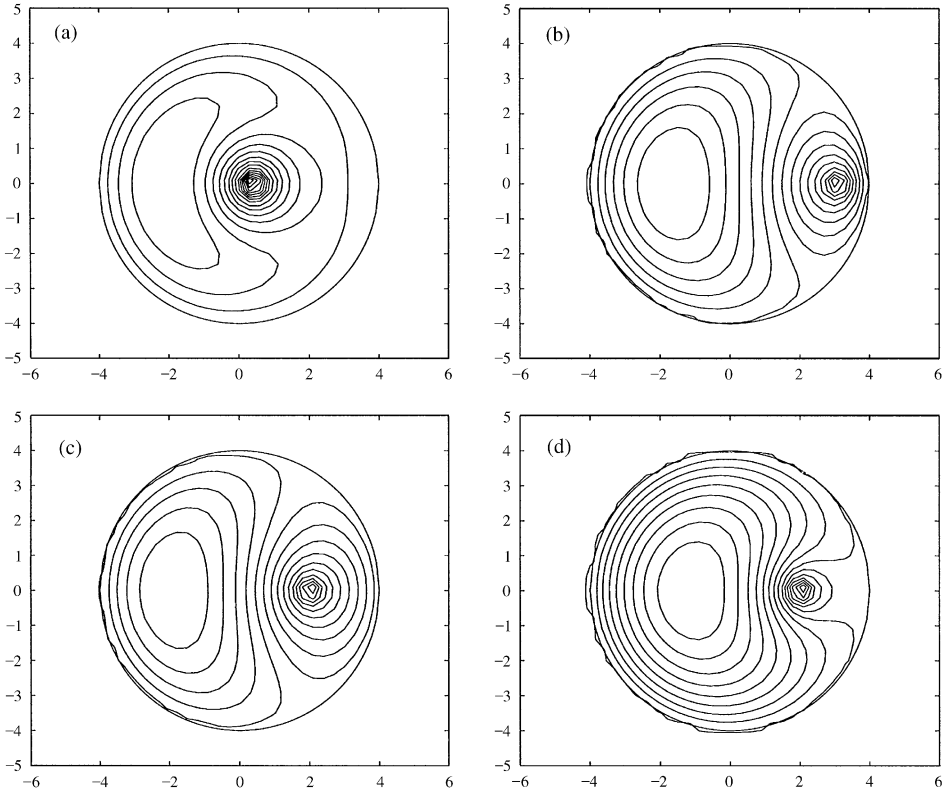

Fig. 1. Flow inside a cylinder induced by a single rotlet for different values of λ_1 and c ($F=1$). (a) $\lambda_1=0.65$, $c=0.4$; (b) $\lambda_1=0.65$, $c=3.0$; (c) $\lambda_1=0.6$, $c=2.0$; (d) $\lambda_1=0.8$, $c=2.0$.

the cylinder towards the wall, first the flow structure of the second kind appears and then the flow structure of the third kind appears. These last two types of structures are shown in Figs. 1(a) and (b) for $c=0.4$ and $c=3$, respectively, where the value of λ_1 is kept fixed at 0.65 (radius of the cylinder, a, is 4). The shape of this eddy changes if value of λ_1 changes with rotlet location c fixed. This is shown in Figs. 1(c) and (d) for $\lambda_1=0.6$ and $\lambda_1=0.8$, respectively, with rotlet location fixed at $c=2.0$.

An attached eddy has been previously observed in [3] with no-slip ($\lambda_1=0$) boundary condition. In the present case, slip parameter λ_1 controls the size of the eddy as shown in this figure. Furthermore, some of the results presented are qualitatively similar to those observed in flows between eccentric rotating cylinders [1].

4.1.2. Pair of opposite rotlets

In Fig. 2, the flow patterns are depicted in the case of a pair of opposite rotlets for several choices of rotlet locations and the value of the slip parameter λ_1. The slip parameter does not change the flow qualitatively as shown in some representative plots in Fig. 2. The flow in all cases consists of two counter-rotating eddies separated by a

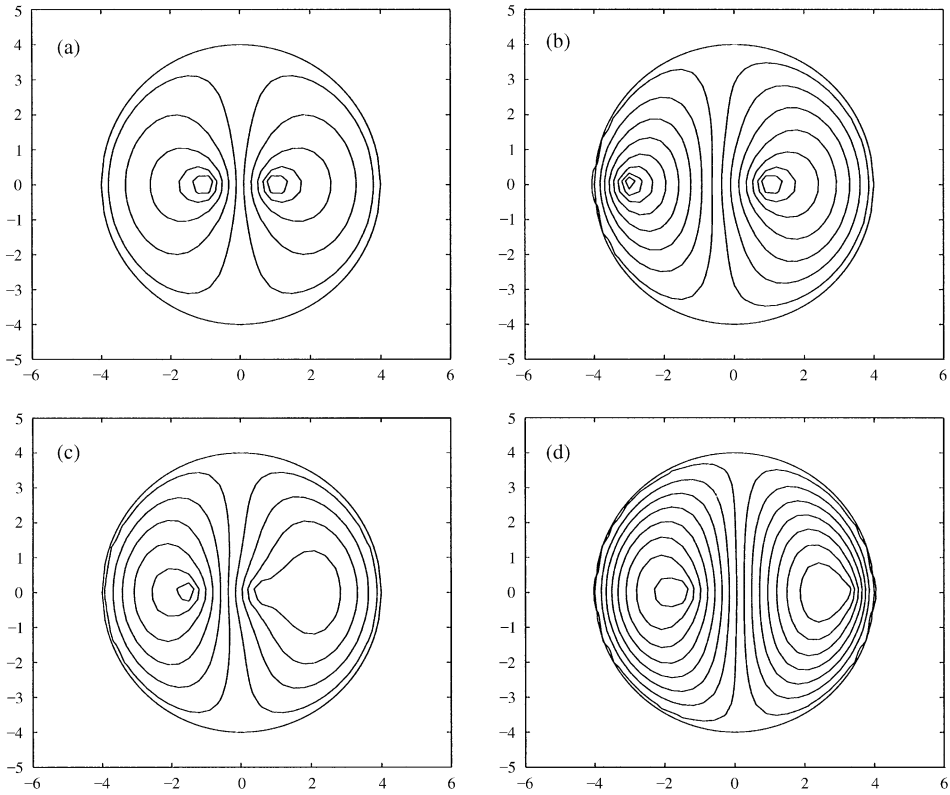

Fig. 2. Flow inside a cylinder generated by a pair of opposite rotlets for different rotlets locations ($F' = -F = 1$). (i) $\lambda_1 = 0.6$: (a) $c = c' = 1.0$; (b) $c = 1.0$, $c' = 3$; (ii) $\lambda_1 = 0.55$; (c) $c = 0.5$, $c' = 1.5$; (d) $c = 3.2$, $c' = 1.5$.

dividing streamline (not shown in these plots) whose end points are stagnation points resting on the wall of the cylinder. The positions of the stagnation points and hence, the position of the dividing streamline, depend on the rotlet locations as well as on the slip parameter. The flow topologies in the present case are very similar to those found in [4] with no-slip boundary conditions.

4.1.3. Pair of equal rotlets

More interesting flow topologies occur in the case of a pair of equal rotlets ($F = F'$). When the rotlets are equidistant from the center along the x-axis, it is found that the distance of the rotlets from the center of the cylinder affects the flow patterns qualitatively which is discussed below through various plots in Figs. 3 and 4. When the rotlets are not equidistant, interesting flow patterns emerge as the location of one of the rotlets changes while the other one is kept fixed. This is discussed below through Fig. 5.

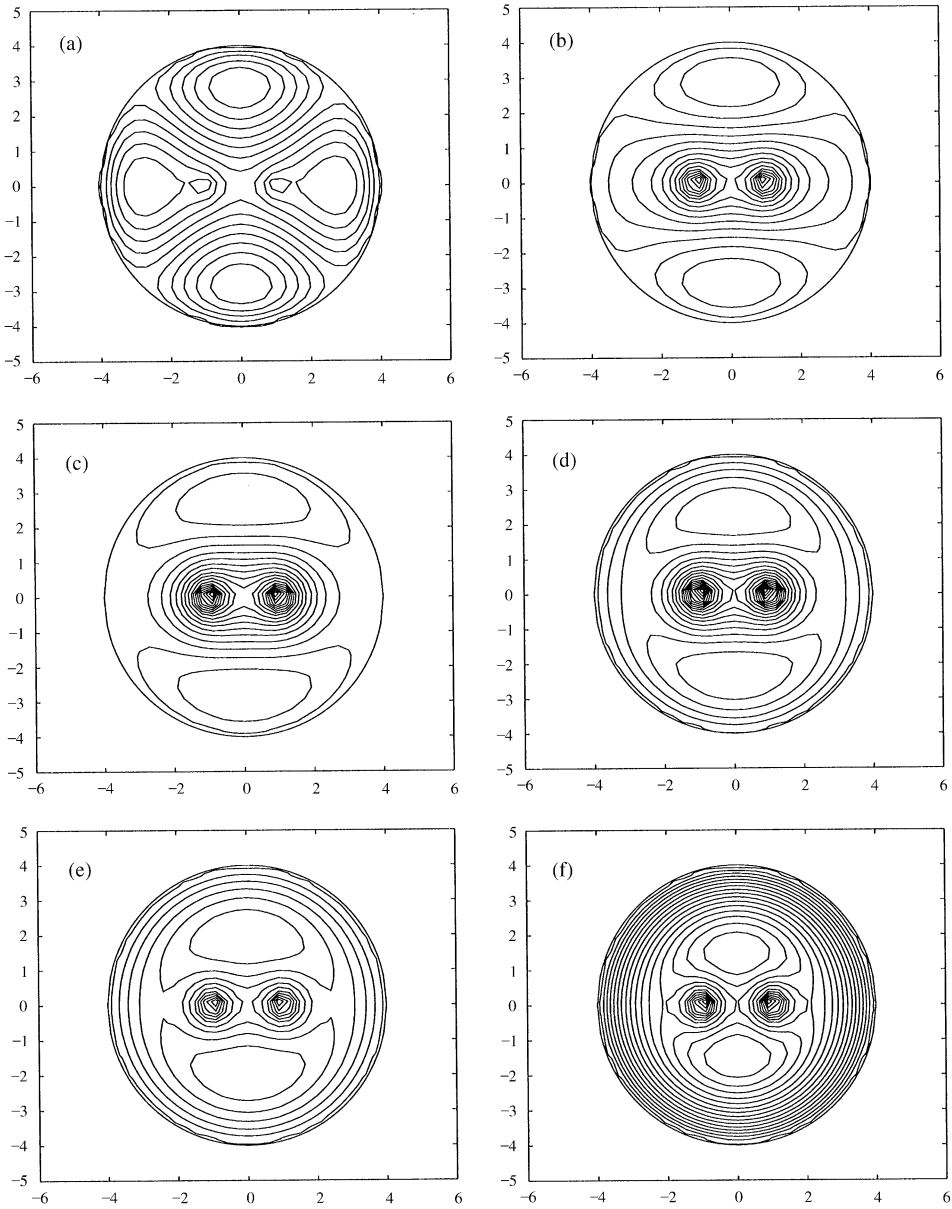

Fig. 3. Flow inside a cylinder induced by a pair of equal rotlets ($F = F' = 1$, $c = c' = 1$) for various values of λ_1. (a) $\lambda_1 = 0.3$; (b) $\lambda_1 = 0.35$; (c) $\lambda_1 = 0.42$; (d) $\lambda_1 = 0.59$; (e) $\lambda_1 = 0.7$; (f) $\lambda_1 = 0.8$.

Fig. 3 above shows streamline patterns for the case of equidistant ($c = c'$) rotlets for several choices of λ_1 with $c = 1$. For small values of λ_1, a single 'large eddy' enclosing the two rotlets and a symmetric pair of eddies outside this large eddy appear as shown in Fig. 3(a) for $\lambda_1 = 0.3$. Initially the large eddy extends up to the wall as

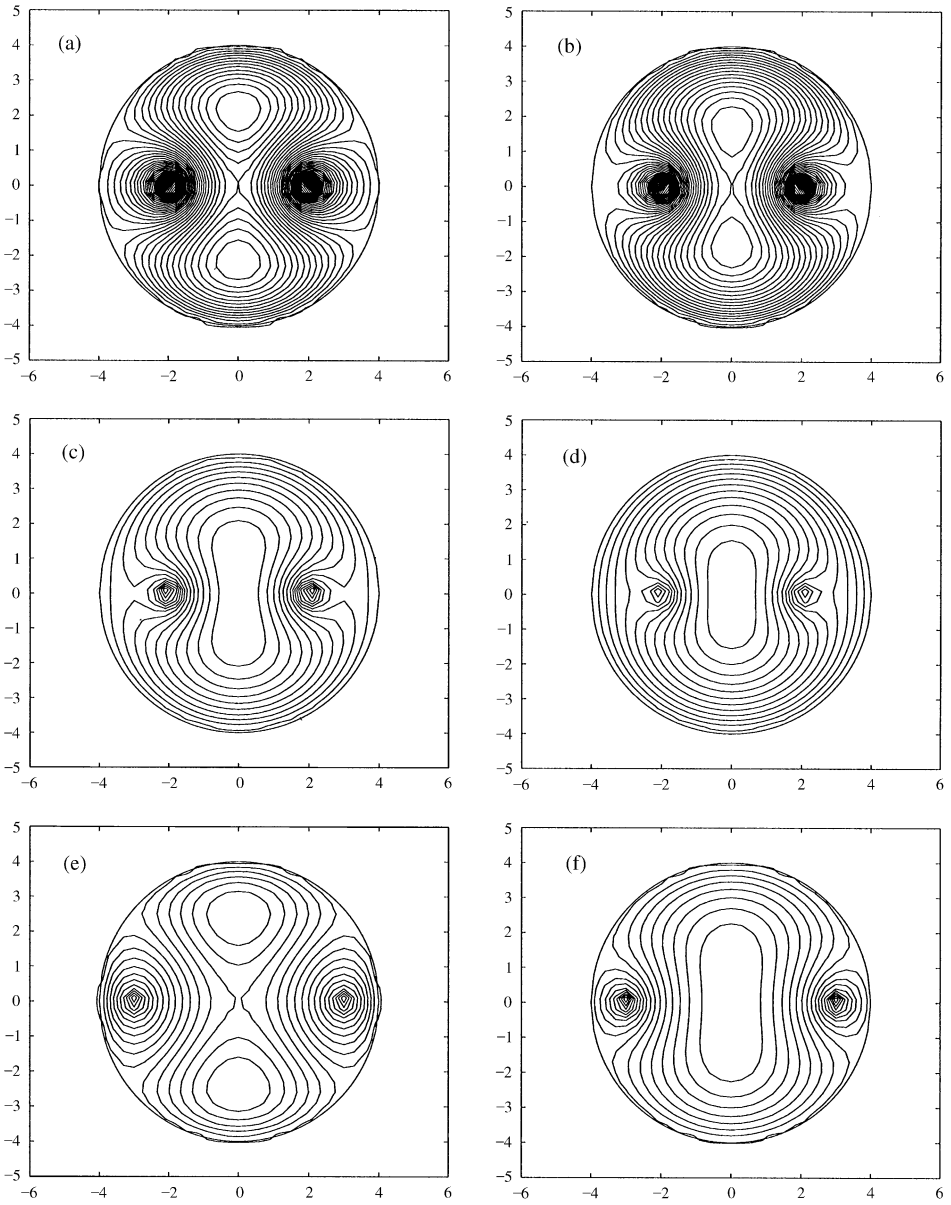

Fig. 4. Flow inside a cylinder generated by a pair of equal rotlets for various values of λ_1 ($F = F' = 1$). (i) $c = c' = 2$: (a) $\lambda_1 = 0.55$; (b) $\lambda_1 = 0.6$; (c) $\lambda_1 = 0.7$; (d) $\lambda_1 = 0.8$; (ii) $c = c' = 3$: (e) $\lambda_1 = 0.45$; (f) $\lambda_1 = 0.6$.

seen in this diagram. As λ_1 increases, these eddies gradually change in shape and size. In particular, the 'large eddy' first shrinks at its farthest near the wall and then starts shrinking while moving inward towards the center. Some of this scenario is shown in Figs. 3(a)–(c). Fig. 3(c) is for $\lambda_1 = 0.42$ when almost circular streamlines concentric

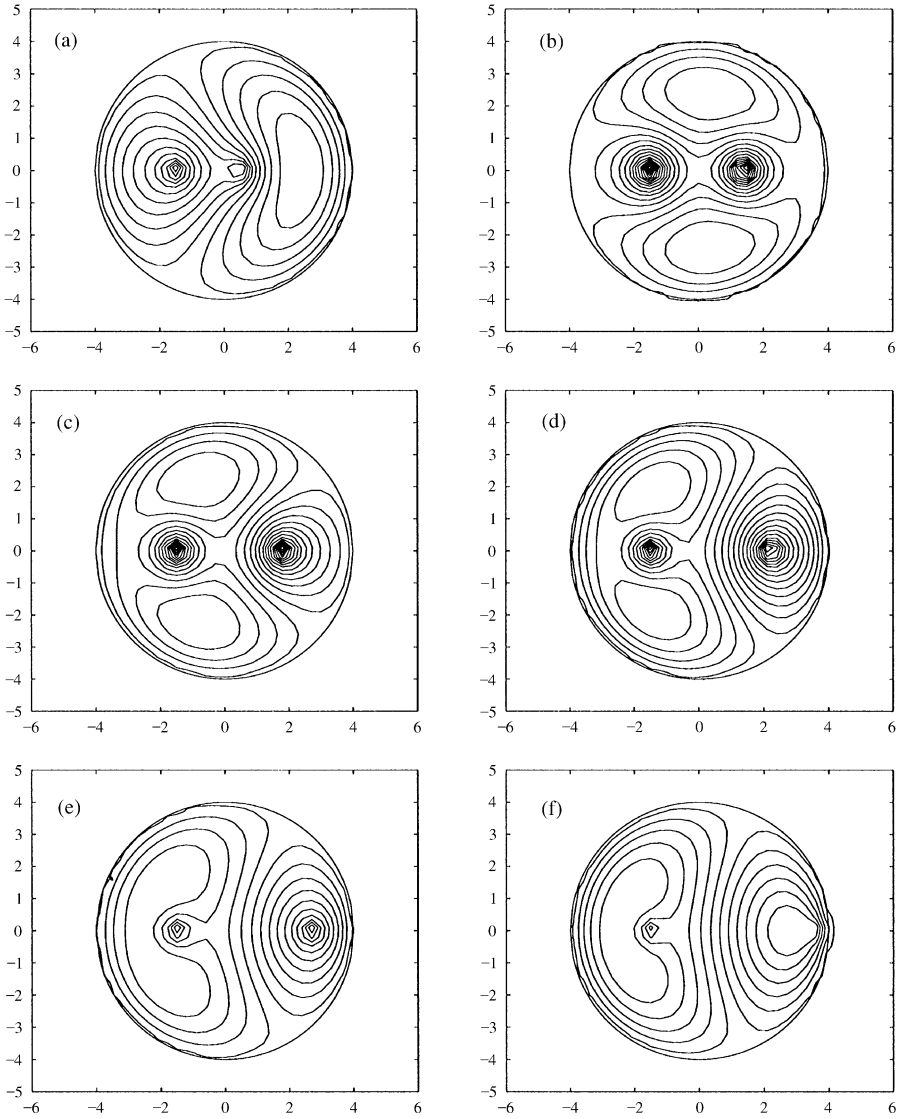

Fig. 5. Flow induced by a pair of equal rotlets inside a cylinder for various values of c ($F = F' = 1$). The right rotlet is at ($r = c,\ \theta = 0$) where (a) $c = 0.5$; (b) $c = 1.4$; (c) $c = 1.8$; (d) $c = 2.2$; (e) $c = 2.7$; (f) $c = 3.7$. For all these cases, $\lambda_1 = 0.6$, and the left rotlet is fixed at ($c' = 1.5,\ \theta = 0$).

with the cylinder first arise near the wall which are not seen in this figure. Further increase of λ_1 has the following effects ongoing simultaneously as shown in Figs. 3(d)–(f): (i) more of the outer region of the flow near the wall becomes circulatory around the center; (ii) the symmetric eddies move towards the center of the cylinder thereby squeezing the middle part of the 'larger eddy', and (iii) the 'larger eddy' even shrinks more inward towards the center while being squeezed thin at the center at the same

time. This process continues with increasing values of λ_1 until the symmetric eddies connect at the center giving birth of a double homoclinic orbit and a stagnation point at the center. This also causes the 'larger eddy' to separate into two smaller eddies each around the rotlets. This is shown in Fig. 3(f). It is worth noting in this figure that three distinct flow regions namely, the circulatory flow in the outer region, the eddies around the rotlets and the rest of the flow region (consisting of two connected symmetric eddies), are separated from each other by a closed separatrix connecting two interior stagnation pints which are equidistant from the center. Two such interior stagnation points also exist in Figs. 3(c)–(e) which are connected by a streamline that separates the two outer symmetric eddies from the interior 'larger eddy' and outer circulatory flow near the wall. This separatrix and two interior stagnation points are not shown in these figures.

Intuitively, flow patterns similar to the ones shown in Fig. 3 and their dependence on λ_1 may be expected for other choices of c, though not necessarily at the same values of λ_1. However, on exploring the flow patterns for various values of c we find that this is not entirely the case. This is shown through a typical case in Figs. 4(a)–(d) where some flow patterns when the rotlets are little farther away ($c=2$) from the center are shown. Subtle differences in flow patterns between Figs. 3 and 4 are obvious. For example, flow pattern in Fig. 3(b) appears to be qualitatively similar to the pattern in Fig. 4(a) when rotated by 90°. However, the changes in patterns with increasing λ_1 in Fig. 3 appears to be similar to that in Fig. 4 only in the region from the wall up to the rotlets. However, it is different in the interior part of the flow region. For example, compare the Figs. 3(f) and 4(c). Each of these has a separatrix that wraps around both the rotlets. The flow between this separatrix and the wall are qualitatively similar. However the interior flow near the center of the cylinder is different. Now, it is not difficult to visualize the kind of flow patterns that should emerge as rotlets are moved farther away from the center and closer to the wall. One such scenario is shown in Figs. 4(e)–(f) where $c=3$. The flow topologies observed here are qualitatively similar to the fluid motion in vortex mixing flows [2]. Further, the existence of homoclinic orbits suggests that the such Stokes flows with partial slip discussed here may be very good candidates for studying chaotic advection. Additionally, the presence of slip might exhibit more interesting and richer variety of dynamical features than those found in [10,6].

A richer and interesting variety of flow patterns emerge when rotlets are placed non-equidistant from the center. Fig. 5 shows a sequence of flow patterns when the right-side rotlet is gradually moved away from the center with the left rotlet kept fixed at a distance $c'=1.5$. All patterns shown pertain to $\lambda_1=0.6$. In Figs. 5(a) and (b), right-side rotlet is closer to the center (i.e., $c/c'<1$) where as in Figs. 5(c)–(f), right-side rotlet is farther from the center (i.e., $c/c'>1$). In each of these cases, one or more separatrices exist which divide the flow region into one or more distinct flow subregions with different qualitative flow features. Each of these subregions contain eddies (circulating flow) which change in size and shape as value of c/c' gradually changes.

In Fig. 5(a), eddy on the right is separated from the eddy containing the two rotlets on its left by a separatrix which is not shown in this figure. When the right eddy is moved farther from the center and c/c' is less than but close to one, the right eddy splits into two surrounded by recirculating streamlines which are separated from the flow surrounding the two rotlets. In this case, two eddies are tilted slightly to the right of the center line perpendicular to the axis containing the center and the two rotlets. This is shown in Fig. 5(b). When $c/c' = 1$, i.e., the rotlets are equidistant, the flow pattern which is not shown here is qualitatively similar to the pattern shown in Fig. 3(c). As soon as c/c' exceeds one, the flow pattern qualitatively similar to the mirror image of the one in Fig. 5(b) about the center line first appears. This is seen in Fig. 5(c) where $c = 1.8$ ($c' = 1.5$). Moving the right rotlet farther away from the center towards the cylinder results in patterns shown in Figs. 5(d)–(f). In all these cases, attached eddies and separatrices (which are either a heteroclinic or double homoclinic orbit) appear. A rigorous mathematical study might further elucidate the flow topologies observed here which we do not pursue here.

If the value of λ_1 is gradually changed in each of the cases shown in Fig. 5, then an altogether different sequence of flow patterns, perhaps more interesting, will emerge just as we saw in Figs. 3 and 4 where the rotlets were equidistant. However, we do not pursue this study here and may be taken up in a later study.

An insight into much of the qualitative features of the flow patterns can be obtained directly from knowing the locations of the stagnation points and their movements as the rotlet positions and the slip parameter are varied. In our case, this can be done more rigorously if desired since the velocity field can be explicitly represented in closed form which contains a definite integral whose evaluation requires some amount of computation. In order to provide a guide towards such a study for flows involving two rotlets, we carry out below a similar study for the one rotlet case.

It is easy to calculate the velocity field due to a rotlet at $(c, 0)$ whose components q_r and q_θ are given by

$$q_r = -F\left[\frac{c\sin\theta}{R_1^2} - \frac{a^2\sin\theta}{cR_2^2} - \frac{1}{\lambda_1 r}\left(1-\frac{r^2}{a^2}\right) r^{(1-\lambda_1)/\lambda_1} \times \int_0^r \rho^{(\lambda_1-1)/\lambda_1}\left(\frac{a^2\sin\theta}{cR_{1\rho}^2} - \frac{2(\rho - a^2/c\cos\theta)a^2\rho\sin\theta}{cR_{1\rho}^4}\right)\mathrm{d}\rho\right], \quad (4.10)$$

$$q_\theta = F\left[\frac{r - c\cos\theta}{R_1^2} - \frac{r - a^2/c\cos\theta}{R_2^2} - \frac{1}{(1-\lambda_1)}\frac{r}{a^2} - \frac{2r}{a^2} r^{(1-\lambda_1)/\lambda_1} I_1 + \left(1-\frac{r^2}{a^2}\right)\frac{\partial}{\partial r}\left(r^{(1-\lambda_1)/\lambda_1} I_1\right)\right]. \quad (4.11)$$

The variation of surface velocity q_θ on the upper half of the cylinder ($0 \leqslant \theta \leqslant \pi$) with θ is shown in Fig. 6(a) for various values of λ_1 with the rotlet location fixed at $c = 2$. It is seen that a stagnation point exits near $\pi/2$ for $\lambda_1 = 0.45$ and gradually

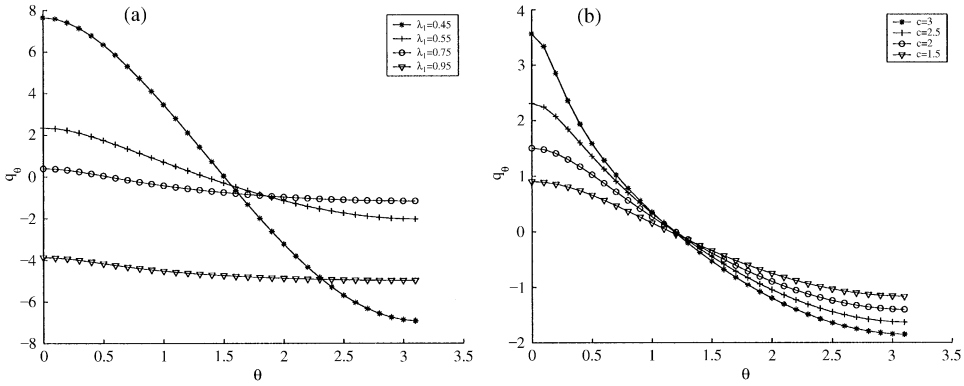

Fig. 6. Fluid velocity on the surface of a cylinder of radius $a=4$ due to a rotlet at $(c,\ \theta=0)$: (a) effect of slip with fixed $c=2.0$; (b) effect of different rotlet location c for a fixed $\lambda_1=0.6$.

moves towards $\theta=0$ with increasing values of λ_1. It is seen from this figure that the stagnation point on the surface is very near the line $\theta=0$ when $\lambda_1=0.75$. At a critical value $\lambda_1=\lambda_c$ (approximately 0.82), this stagnation point on the cylinder surface is exactly at $(r=a,\ \theta=0)$ on the surface of the cylinder, and with further increase in the value of λ_1, this stagnation point leaves the surface of the cylinder and moves inward along the $\theta=0$ line. Therefore we see in Fig. 6(a) that there is no stagnation point on the surface of the cylinder above a certain value of λ_1. In fact we see in this figure that the surface velocity changes very little at $\lambda_1=0.95$. In fact this is so for almost all values of $\lambda_1>\lambda_c$. Therefore, it is natural to expect circulatory flow near the cylinder for $\lambda_1>\lambda_c$ and this region grows in size with increasing λ_1. This is consistent with the flow patterns that we have shown in Fig. 1.

Fig. 6(b) shows plots of q_θ against θ for several choices of c (rotlet locations) with λ_1 fixed at 0.6. Similar to the above, we can use these plots to draw some inferences about qualitative similarities or differences between the flow features for various values of c. For example, it is quite clear from these plots that a stagnation point exists on the upper (as well as lower) surface in each case whose location changes very little with the rotlet location. Moreover, the surface velocity do not change as drastically with c for fixed λ_1 as it did with λ_1 for a fixed c. These observations are perhaps an indication of the fact that the flow patterns are likely to be simple and change little in a qualitative sense with changes in the rotlet location. This is consistent with our earlier observation in Fig. 1.

4.2. Source inside a circular cylinder

The stream function for a potential source located at $r=c<a,\ \theta=0$, in the absence of a cylinder is given by

$$\psi_0=S\tan^{-1}\left(\frac{r\sin\theta}{c-r\cos\theta}\right).$$

For $r > c$, above expression may be expanded in the form

$$\psi_0 = S\sum_{n=1}^{\infty} \frac{c^n}{nr^n} \sin n\theta \,. \tag{4.12}$$

From (3.1) and (4.12), we obtain

$$G(r) = 0, \quad \alpha_n = \frac{Sc^n}{n}, \quad \beta_n = 0 \quad \text{for all } n \geqslant 1.$$

Since $G(r) = 0$, the coefficients A_0, B_0 vanish in the present case. The coefficients A_n, B_n, $n \geqslant 1$ for a source flow after the introduction of a cylinder are

$$A_n = -\frac{1}{n\lambda_1 - 1 + \lambda_1}\left[(n+1)(1-\lambda_1)\frac{\alpha_n}{a^{2n}}\right],$$

$$B_n = \frac{1}{n\lambda_1 - 1 + \lambda_1}\left[\frac{n\alpha_n}{a^{2n+2}}\right]. \tag{4.13}$$

As in the rotlet problem, Fourier series solution with the constants given in (4.13) may be summed to yield the following closed form expression:

$$\psi(r,\theta) = S\left\{\tan^{-1}\left(\frac{r\sin\theta}{c - r\cos\theta}\right) - \tan^{-1}\left(\frac{a^2\sin\theta}{rc - a^2\cos\theta}\right) - \frac{(r^2 - a^2)}{c\lambda_1} r^{(1-\lambda_1)/\lambda_1} I_2\right\}, \tag{4.14}$$

where

$$I_2 = \frac{1}{\lambda_1}\int_0^r \rho^{(\lambda_1 - 1)/\lambda_1} \frac{\sin\theta}{R_{1\rho}^2}\, \mathrm{d}\rho \,. \tag{4.15}$$

This solution does not seem to have been derived in the literature before. In the limit $\lambda_1 \to 1$, the above solution reduces to

$$\psi(r,\theta) = S\left\{\tan^{-1}\left(\frac{r\sin\theta}{c - r\cos\theta}\right) - \frac{r^2}{a^2}\tan^{-1}\left(\frac{a^2\sin\theta}{rc - a^2\cos\theta}\right)\right\}. \tag{4.16}$$

This solution corresponds to a source located inside a stress-free circular cylinder. The physical significance of this solution is not available at this time.

The solution for a source of strength S' located at (c', π) inside a cylinder is

$$\psi(r,\theta) = S'\left\{\tan^{-1}\left(\frac{r\sin\theta}{c' + r\cos\theta}\right) - \tan^{-1}\left(\frac{a^2\sin\theta}{rc' + a^2\cos\theta}\right) - \frac{(r^2 - a^2)}{c'} r^{(1-\lambda_1)/\lambda_1} I_2'\right\}, \tag{4.17}$$

where

$$I_2' = \frac{1}{\lambda_1}\int_0^r \rho^{(\lambda_1 - 1)/\lambda_1} \frac{\sin\theta}{R_{1\rho}'^2}\, \mathrm{d}\rho \,, \tag{4.18}$$

and $R_{1\rho}'^2$ is as defined in (4.9).

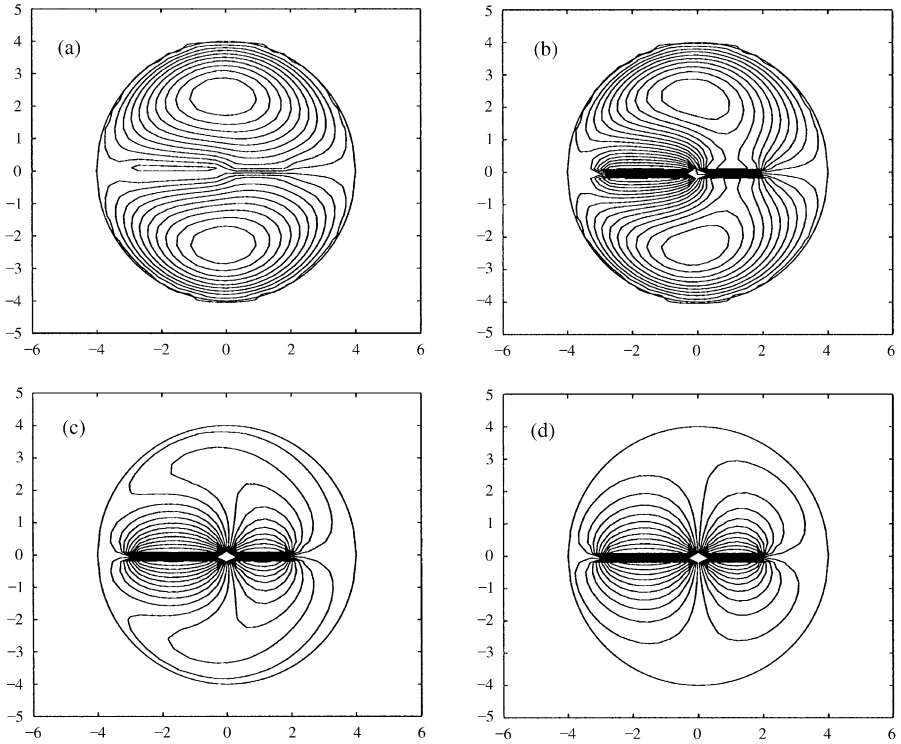

Fig. 7. Flows generated by a source at ($c=2$, $\theta=0$) and a sink at ($c'=3$, $\theta=\pi$) inside a cylinder for various values of λ_1. Here $S=1$, $S'=-1$. (a) $\lambda_1=0.4$; (b) $\lambda_1=0.45$; (c) $\lambda_1=0.55$; (d) $\lambda_1=0.9$.

Figs. 7(a)–(d) show flow patterns for an increasing sequence of values of λ_1 when a source and a sink are located at distances $x=2$ and $x=-3$, respectively. First, a symmetric pair of secondary eddies appears with their centers almost aligned on the y-axis. This is shown in Fig. 7(a) for $\lambda_1=0.4$. With increasing values of λ_1, these eddies tilt to the right and start moving towards the line joining the source and the center of the cylinder. Fig. 7(b) shows this for a typical value of $\lambda_1=0.45$. A small flow region near the line joining the sink and the center of the cylinder ensues where the fluid seems to flow from the center to the sink. Rest of the flow seems to contain a recirculating zone surrounded by fluid flowing from the source to the center. With further increases in the value of λ_1, the flow region between the center and the sink grows in size where as the rest of the flow region shrinks in size as seen in Fig. 7(c) for $\lambda_1=0.55$. Eventually, at $\lambda_1=0.9$, a dipole-type flow ensues at the origin.

If a source and a sink are located equidistant ($c=c'=2$) from the center along a diagonal, then the flow structure (See Figs. 8(a)–(b)) changes little. An increase in the value of λ_1 in this case pushes the eddies towards the wall. It is worth mentioning here that Lord Rayleigh [5] found no secondary flow in the case of a source and a sink located diagonally opposite on the surface of a cylinder. Lord Rayleigh [5] also pointed out that inertial terms are necessary to have secondary flows. Contrary to his

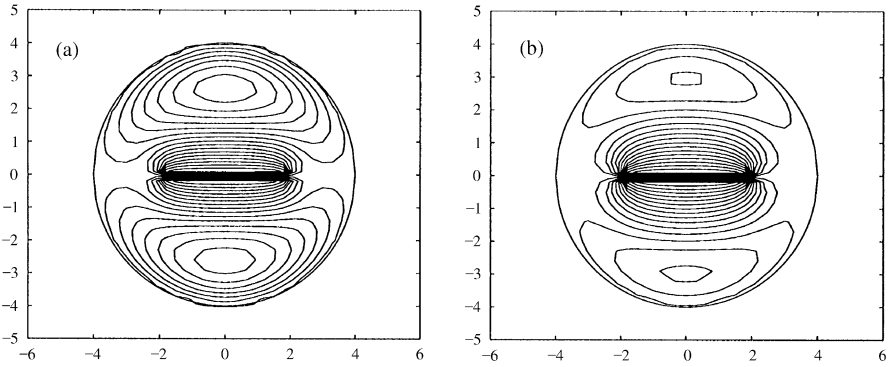

Fig. 8. Flows generated by a source at $(c=2,\ \theta=0)$ and sink at $(c'=2,\ \theta=\pi)$ for various values of λ_1 $(S=1,\ S'=-1)$. (a) $\lambda_1=0.2$; (b) $\lambda_1=0.4$.

belief, we have shown here that secondary flows can exist in the absence of inertial effects and this is due to the presence of partial slip at the boundary.

The components of velocity field induced by a source located at $(c,0)$ inside a cylinder are given by

$$q_r=-S\left\{\frac{c\cos\theta-r}{R_1^2}+\frac{a^2}{c^2}\frac{(a^2-rc\cos\theta)}{rR_2^2}-\frac{(r^2-a^2)}{cr\lambda_1}r^{(1-\lambda_1)/\lambda_1}\right.$$
$$\left.\times\int_0^r\rho^{(\lambda_1-1)/\lambda_1}\left[\frac{\cos\theta}{R_{1\rho}^2}-\frac{2\rho^2\sin^2\theta}{R_{1\rho}^4}\right]\mathrm{d}\rho\right\}, \tag{4.19}$$

$$q_\theta=S\left\{\frac{c\sin\theta}{R_1^2}-\frac{a^2\sin\theta}{cR_2^2}-\frac{2r}{c}r^{(1-\lambda_1)/\lambda_1}I_2-\frac{r^2-a^2}{c}\frac{\partial}{\partial r}(r^{(1-\lambda_1)/\lambda_1}I_2)\right\}. \tag{4.20}$$

Figs. 9(a) and (b) show plots of fluid velocity versus θ on the wall of the cylinder for different values of λ_1 (c fixed) and rotlet location (λ_1 fixed), respectively. It clearly shows, as expected, that only two diagonally opposite stagnation points exist.

One can easily modify this formulae for the cases shown in Figs. 7 and 8 and can draw inferences about some of the qualitative features of the various flow patterns directly from this formulae as we have done for the case of one rotlet in the previous section.

4.3. A line Stokeslet inside a circular cylinder

(i) Stokeslet with its axis along x-direction

Here we consider a Stokeslet of strength F_1 located at $r=c<a$, $\theta=0$. The axis of the Stokeslet is taken to be along the positive x-direction. The stream function for this

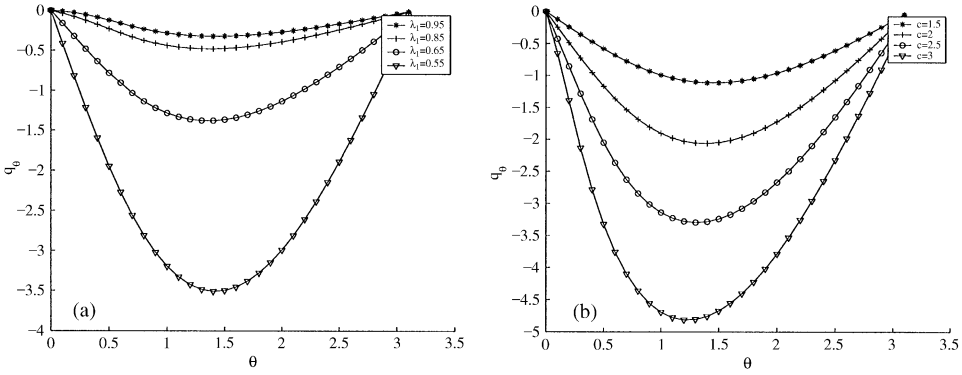

Fig. 9. Fluid velocity on the surface of a cylinder of radius $a=1$ due to a source $(c,\theta=0)$: (a) effect of slip with fixed $c=2.0$; (b) effect of different source location c for a fixed $\lambda_1=0.6$.

Stokeslet in free space is given by

$$\psi_0 = F_1 r \sin\theta \log R_1.$$

The Fourier expansion of ψ_0 may be written as

$$\psi_0 = F_1 r \sin\theta \left(\log r + \frac{c^2}{4r^2}\right) - \frac{F_1}{2}\sum_{n=2}^{\infty}\left[\frac{c^{n-1}}{(n-1)r^{n-2}} - \frac{c^{n+1}}{(n+1)r^n}\right]\sin n\theta\,. \tag{4.21}$$

When the above Stokeslet is inside a cylinder of radius a, the stream function can be found by evaluating the appropriate unknown coefficients in a similar way as explained in the rotlet problem. We skip the details of derivation and give here the final solution for the stream function which takes the form

$$\psi(r,\theta) = F_1 \sin\theta \left[r\log R_1 - r\log\left(\frac{cR_2}{a}\right) + \left(1-\frac{r^2}{a^2}\right)\frac{(c^2-a^2)a^2}{2c^2} r^{(1-\lambda_1)/\lambda_1} I_3\right], \tag{4.22}$$

where

$$I_3 = \frac{1-\lambda_1}{\lambda_1}\int_0^r \rho^{(\lambda_1-1)/\lambda_1}\frac{\sin\theta}{R_{1\rho}^2}\,\mathrm{d}\rho\,. \tag{4.23}$$

The notations R_2, $R_{1\rho}$ are as defined in (4.5a) and (4.5b). The two limiting cases for a rigid cylinder with stick boundary condition and for a shear-free cylinder with perfect slip condition follow from (4.22).

The solution for a Stokeslet of strength F_1' located at (c',π) is

$$\psi(r,\theta) = F_1' \sin\theta \left[r\log R_1' - r\log\left(\frac{c'R_2'}{a}\right) + \left(1-\frac{r^2}{a^2}\right)\frac{(c'^2-a^2)a^2}{2c'^2} r^{(1-\lambda_1)/\lambda_1} I_3'\right], \tag{4.24}$$

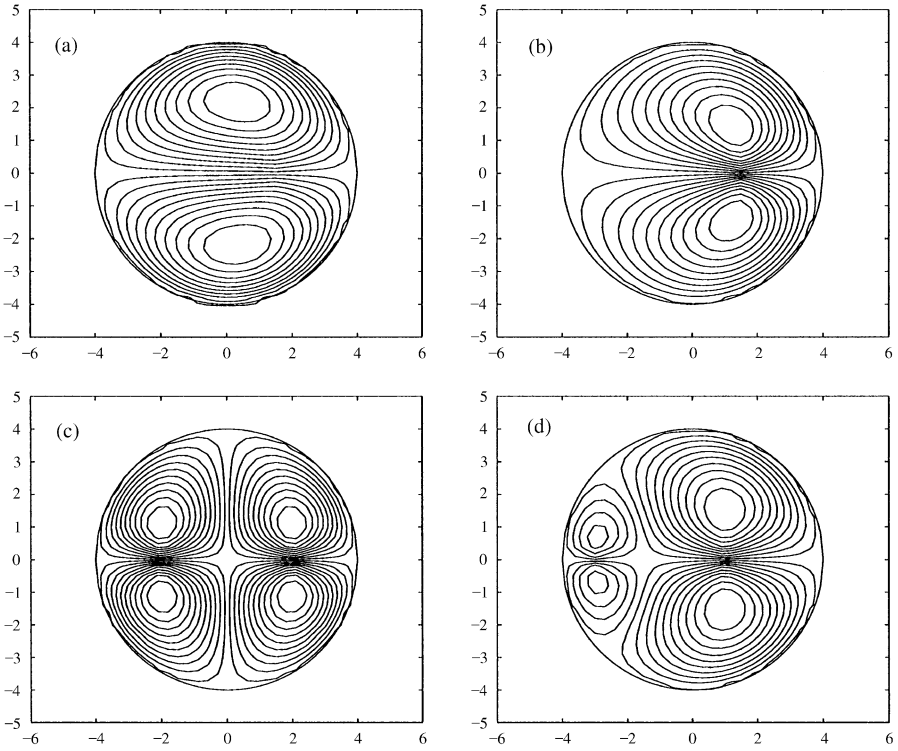

Fig. 10. Stokeslet (with its axis along x-direction) induced flows inside a cylinder for various values of λ_1. (i) Single Stokeslet at ($c=1.5,\ \theta=0$), with $F_1=1$: (a) $\lambda_1=0.6$; (b) $\lambda_1=0.9$; (ii) A pair of opposite Stokeslets (with $F_1=-F_1'=1$): (c) $\lambda_1=0.7,\ c=c'=2$; (d) $\lambda_1=0.7,\ c=1,\ c'=3$.

where

$$I_3'=\frac{1-\lambda_1}{\lambda_1}\int_0^r \rho^{(\lambda_1-1)/\lambda_1}\frac{\sin\theta}{R_{1\rho}'^2}\,\mathrm{d}\rho\,. \tag{4.25}$$

The relations R_2', $R_{1\rho}'$ are the same as defined in (4.9).

Fig. 10 shows the streamline patterns due to Stokeslet induced fluid motions. In the case of a single Stokeslet, a pair of symmetric eddies appears. An increase of λ_1 does not change the pattern significantly as shown in Figs. 10(a) and (b). In the case of a pair of opposite Stokeslets located equidistant from the center on the x-axis, the flow has four identical eddies (see Fig. 10(c)). On the other hand, if the Stokeslets are located at non-equidistance positions, a symmetric pair of smaller and bigger eddies appear (see Fig. 10(c)). The eddies near the Stokeslet which is closer to the wall are smaller, as expected, because the fluid motion created by this Stokeslet suffers a greater resistance from the wall.

Flow patterns shown above may be expected on qualitative ground, but unexpected flow patterns may emerge for some values of λ_1, in particular for large values when the surface condition approaches stress-free condition. Without cluttering with too many

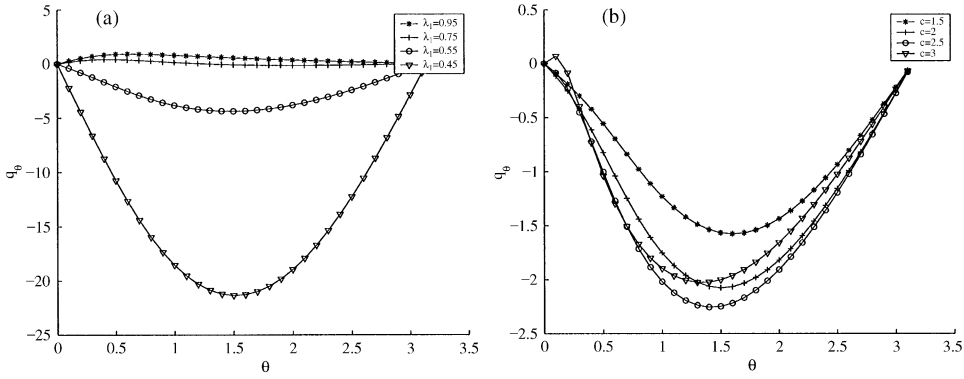

Fig. 11. Fluid velocity on the surface of a cylinder with radius $a=4$ due to a Stokeslet located at $(r=c,\ \theta=0)$ with its axis along x-direction: (a) effect of slip with fixed $c=2.0$; (b) effect of different Stokeslet location c for a fixed $\lambda_1=0.6$.

figures, we show below that such possibilities exist just by computing the fluid velocity on the surface due to a Stokeslet for various choices of the slip parameter.

The velocity components due to a Stokeslet with its axis along x-direction located at $(r,\theta)=(c,0)$ are

$$q_r = -F_1\cos\theta\left(\log R_1 - \log\frac{cR_2}{a}\right) + F_1\sin\theta\left(\frac{rc\sin\theta}{R_1} - \frac{a^2 r\sin\theta}{cR_2}\right) + \frac{1-\lambda_1}{2r\lambda_1}\left(1-\frac{r^2}{a^2}\right)\frac{(c^2-a^2)a^2}{c^2}r^{(1-\lambda_1)/\lambda_1} \times \int_0^r \rho^{(\lambda_1-1)/\lambda_1}\left[\frac{\cos\theta}{R_{1\rho}^2} - \frac{2\rho a^2\sin^2\theta}{cR_{1\rho}^4}\right]\mathrm{d}\rho\,, \tag{4.26}$$

$$q_\theta = F_1\sin\theta\left[\log R_1 + \frac{r(r-c\cos\theta)}{R_1^2} - \log\left(\frac{c}{a}R_2\right) - \frac{r(r-(a^2/c)\cos\theta)}{R_2^2} - r\frac{c^2-a^2}{c^2}r^{(1-\lambda_1)/\lambda_1}I_3\right] + \left(1-\frac{r^2}{a^2}\right)\frac{(c^2-a^2)a^2}{2c^2}\frac{\partial}{\partial r}(r^{(1-\lambda_1)/\lambda_1}I_3)\,. \tag{4.27}$$

Figs. 11(a) and (b) show q_θ against θ on the upper half of the cylinder surface for several values of λ_1 and Stokeslet location, respectively. These plots in Fig. 11(a) show some features which are expected and some which are not. For example, locations of two stagnation points at $\theta=0,\pi$ on the surface for all these flows are expected. On the other hand, the fact that the fluid flow on the surface is counter-clockwise for modest values of λ_1 (see plots for $\lambda_1=0.45,\ 0.55$ in Fig. 11(a)) and clockwise for large values of λ_1 (see plot for $\lambda_1=0.95$ in Fig. 11(a)) is unexpected. This change of flow direction means that there is a threshold value of λ_1 when other stagnation points must arise on the cylinder surface. We see in the plot for $\lambda_1=0.75$, that there is a stagnation point around $\theta=\pi/2$ (and its image on the lower half). It is quite evident that the flows

even with a single Stokeslet can be quite different qualitatively from the ones shown in Figs. 10(a) and (b) for certain choices of λ_1 and c.

(ii) Stokeslet with its axis along y-direction

The stream function for a Stokeslet of strength F_2 with axis along y-direction located at $(r,\theta)=(c,0)$, $c<a$ in an unbounded fluid motion is

$$\psi_0 = -F_2(r\cos\theta - c)\log R_1.$$

The Fourier expansion of ψ_0 for $r>c$ is

$$\psi_0 = F_2\left[\frac{c}{2} + c\log r - r\cos\theta\left(\log r + \frac{3c^2}{4r^2}\right)\right] - \frac{F_2}{2}\sum_{n=2}^{\infty}\left[\frac{c^{n-1}}{(n-1)r^{n-2}} + \left(\frac{1}{n+1} - \frac{2}{n}\right)\frac{c^{n+1}}{r^n}\right]\cos n\theta\,. \tag{4.28}$$

The unknown coefficients in the Fourier series solution for the flow induced by the above Stokeslet within a cylinder of radius a can be found using the steps explained previously in the rotlet problem. The exact solution for the stream function in the present case is

$$\psi(r,\theta) = F_2\left[-(r\cos\theta - c)\log R_1 + (r\cos\theta - c)\log\frac{cR_2}{a}\right. \tag{4.29}$$

$$\left. + \frac{c\lambda_1}{(1-\lambda_1)}\left(1 - \frac{r^2}{a^2}\right) - \left(\frac{r^2}{a^2} - 1\right) r^{(1-\lambda_1)/\lambda_1} I_4\right]\,, \tag{4.29}$$

where

$$I_4 = c\left(1 - \frac{(1-\lambda_1)}{2\lambda_1}\frac{(a^2-c^2)}{c^2}\right)\int_0^r \rho^{(\lambda_1-1)/\lambda_1}\frac{\rho - a^2/c\cos\theta}{R_{1\rho}^2}\,\mathrm{d}\rho\,. \tag{4.30}$$

In the limit $\lambda_1 \to 0$, (4.29) yields the solution for a Stokeslet-cylinder combination with stick (no-slip) boundary conditions. When $\lambda_1 \to 1$, Eq. (4.29) reduces to the solution for a shear-free cylinder.

The solution for a Stokeslet of strength F_2' located at (c',π) inside the cylinder of radius a is easily seen to be

$$\psi(r,\theta) = F_2'\left[(r\cos\theta + c')\log R_1 - (r\cos\theta + c)\log\frac{c'R_2}{a} + \frac{c'\lambda_1}{(1-\lambda_1)}\left(1 - \frac{r^2}{a^2}\right)\right. - \left.\left(\frac{r^2}{a^2} - 1\right)c'\left(1 - \frac{(1-\lambda_1)}{2\lambda_1}\frac{(a^2-c'^2)}{c'^2}\right) r^{(1-\lambda_1)/\lambda_1} I_4'\right]\,, \tag{4.31}$$

where

$$I_4' = c'\left(1 - \frac{(1-\lambda_1)}{2\lambda_1}\frac{(a^2-c'^2)}{c'^2}\right)\int_0^r \rho^{(\lambda_1-1)/\lambda_1}\frac{\rho + a^2/c'\cos\theta}{R_{1\rho}'^2}\,\mathrm{d}\rho\,. \tag{4.32}$$

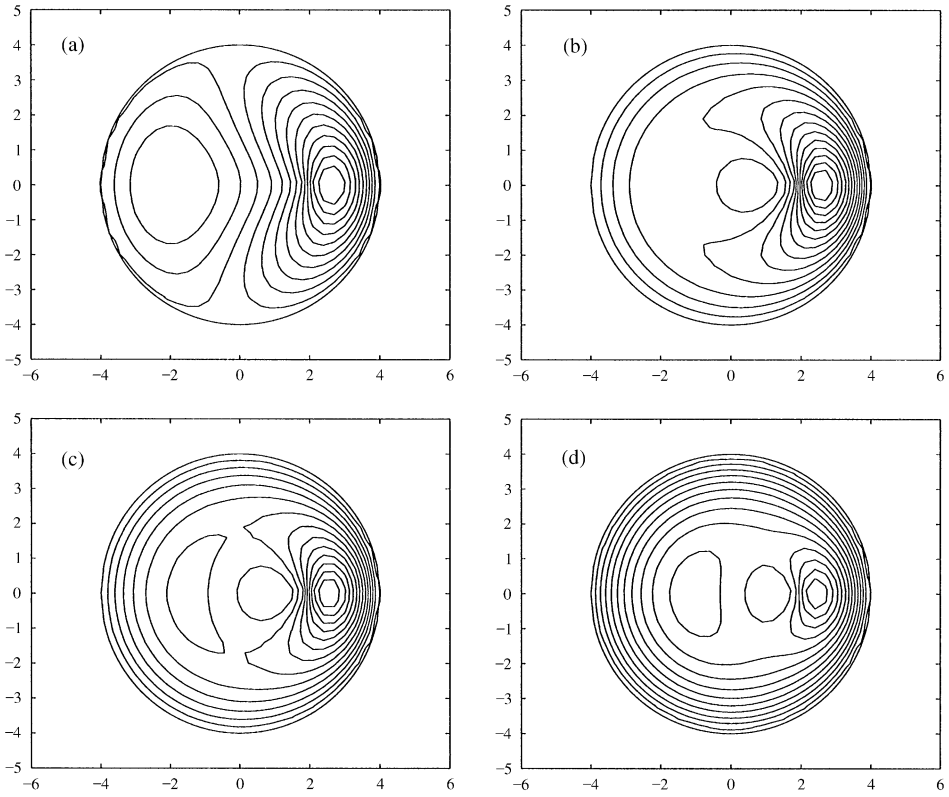

Fig. 12. Flow due to a Stokeslet with its axis along y-direction located at ($c = 2.0$, $\theta = 0$) inside a cylinder for different values of λ_1: (a) $\lambda_1 = 0.53$; (b) $\lambda_1 = 0.63$; (c) $\lambda_1 = 0.67$; (d) $\lambda_1 = 0.75$.

In Fig. 12, some flow patterns are shown for a single Stokeslet with its axis along y-direction for several values of λ_1. A pair of attached eddies of unequal size appears in the flow domain for $\lambda_1 = 0.53$ (see Fig. 12(a)). One of these appears in the vicinity of the Stokeslet and the other one appears far from it. At this value, there is a pair of stagnation points on the cylinder: one on the upper half of the cylinder, and the other one on the lower half. This can be seen in the surface velocity plot in Fig. 14(a). These velocity plots show that these stagnation points move towards the point ($r = a$, $\theta = 0$) on the surface with increasing values of λ_1, it would appear that these two will perhaps collide at the point ($r = a$, $\theta = 0$) as $\lambda_1 \to 1$. As seen from the plots in Figs. 12(b)–(d), with increasing values of λ_1, two attached eddies move inward with their sizes shrinking, and the fluid near the cylinder wall exhibits circulatory motion. We see, in Figs. 12(c) and (d) that another set of eddies appears in the neighborhood of the origin.

Some streamlines for a pair of Stokeslets are sketched in Fig. 13 for several values of λ_1. These figures show appearance of an eddy in the vicinity of each Stokeslet. In Figs. 13(a)–(c), Stokeslet locations which are placed equidistant from the center on the x-axis do not change ($c = c' = 1.5$). Here we see that a third eddy also occurs

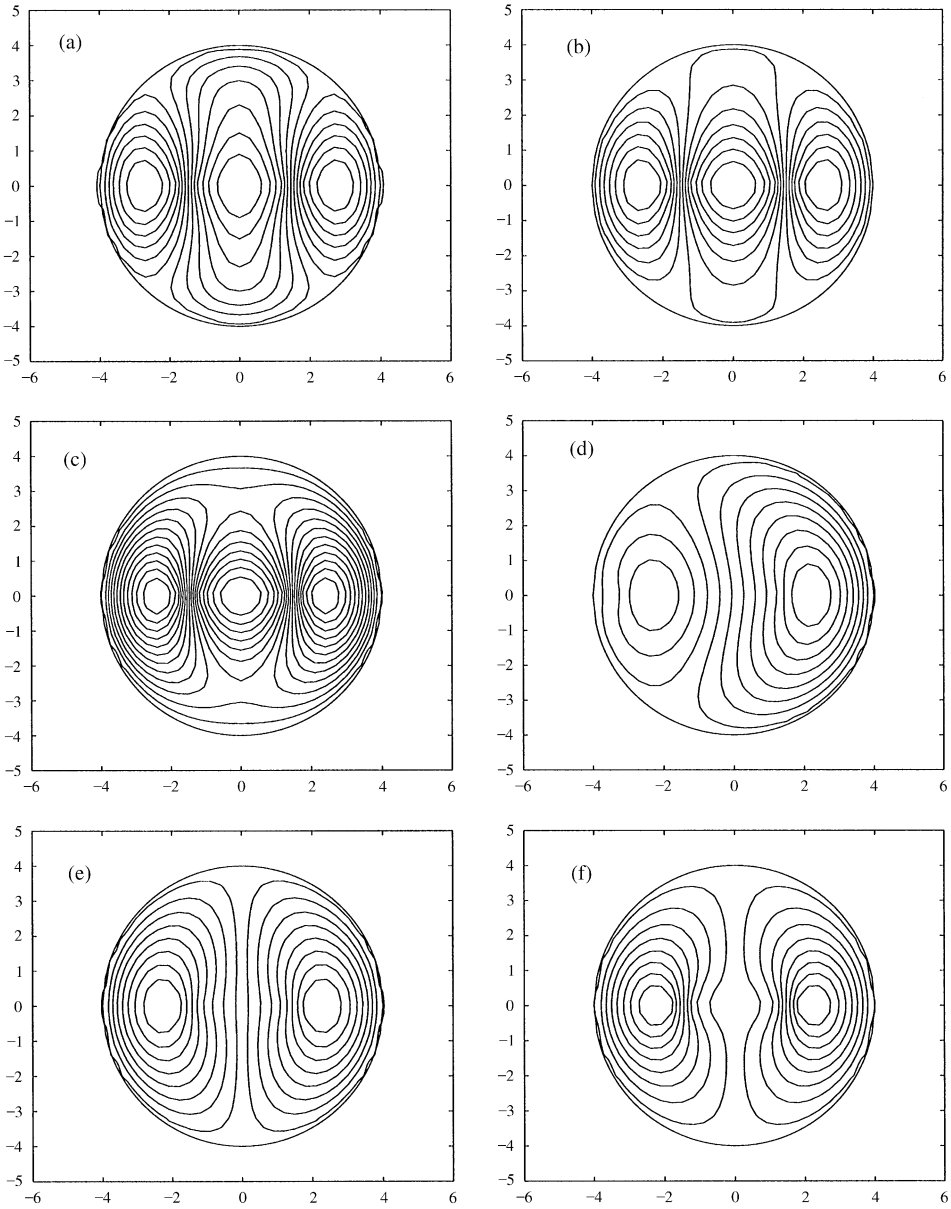

Fig. 13. Flows inside a cylinder induced by a pair of Stokeslets with their axes along y-direction. (i) Equal Stokeslets ($F_2 = F_2' = 1$), $c = c' = 1.5$ in figures (a)–(c): (a) $\lambda_1 = 0.45$; (b) $\lambda_1 = 0.55$; (c) $\lambda_1 = 0.6$; (d) $\lambda_1 = 0.6$ (Here $c = 1.5$, $c' = 3.0$); (ii) Opposite Stokeslets ($F_2 = -F_2' = 1$), $c = c' = 1.5$: (e) $\lambda_1 = 0.7$; (f) $\lambda_1 = 0.9$.

surrounding the origin. The shapes of these eddies change little, but their sizes shrink with increasing λ_1. Further increase of the slip parameter shrinks the size of the eddies and creates a circulatory motion near the wall (Fig. 13(c)) which encloses all three eddies. Fig. 13(c) shows this at a value of $\lambda_1 = 0.6$. Flow patterns could be quite

different qualitatively from the above if one of the Stokeslets is moved farther out or has strength of opposite sign. This is shown in Fig. 13(d) which has the same value of λ_1 as in Fig. 13(c), except that the Stokeslet on the left is moved farther out towards the wall. Flow patterns for two opposite Stokeslets located equidistant from the center are shown in Figs. 13(e) and (f). Here locations are the same as in Figs. 13(a)–(c) but strengths of the Stokeslets are of opposite sign. Here, we see that the flow topologies are quite different from the ones in Figs. 13(a)–(c) and look very similar to the patterns for a single Stokeslet shown previously.

The velocity components in r and θ directions due to a Stokeslet at $(c,0)$ are given by

$$q_r = F_2 \left[-\sin\theta \log R_1 + (r\cos\theta - c)\frac{c\sin\theta}{R_1^2} + \sin\theta \log\left(\frac{cR_2}{a}\right) \right.$$
$$-(r\cos\theta - c)\frac{a^2\sin\theta}{cR_2^2} - \left(\frac{r^2}{a^2} - 1\right)\frac{c}{r}\left(1 - \frac{(1-\lambda_1)}{2\lambda_1}\frac{(a^2-c^2)}{c^2}\right) r^{(1-\lambda_1)/\lambda_1}$$
$$\left. \times \int_0^r \rho^{(\lambda_1-1)/\lambda_1}\left(\frac{a^2\cos\theta}{R_{1\rho}^2} - \frac{(\rho - \frac{a^2}{c}\cos\theta)a^2\rho\sin\theta}{cR_{1\rho}^4}\right) \mathrm{d}\rho \right], \tag{4.33}$$

$$q_\theta = -F_2 \left\{ \cos\theta \log R_1 + (r\cos\theta - c)\frac{(r - c\cos\theta)}{R_1^2} - \cos\theta \log\frac{cR_2}{a} \right.$$
$$-(r\cos\theta - c)\frac{(r - (a^2/c)\cos\theta)}{R_2^2} - \frac{2cr\lambda_1}{1-\lambda_1}$$
$$\left. -\frac{2r}{a^2} r^{(1-\lambda_1)/\lambda_1} I_4 - \left(\frac{r^2}{a^2} - 1\right)\frac{\partial}{\partial r}(r^{(1-\lambda_1)/\lambda_1} I_4) \right\}. \tag{4.34}$$

The plots of q_θ versus θ for the upper half of the surface for different values of the slip parameter and Stokeslet location are shown in Figs. 14(a) and (b) respectively. In Fig. 14(a), Stokeslet location is fixed at $c=2$ and in Fig. 14(b), value of λ_1 is fixed at 0.6. It is seen in Fig. 14(a) that there is a stagnation point on the upper half (and also one on the lower half) of the cylinder surface which moves towards the point $(r=a,\ \theta=0)$ on the surface as the value of λ_1 gradually increases. This causes crowding of the streamlines in Figs. 12(a)–(d) at the vicinity of the point $(r=a,\ \theta=0)$ on the cylinder surface. This stagnation point however may not exist for all choices of c and λ_1. This can be seen in one of the plots in Fig. 14(b) where similar plots are shown for several locations $(c,0)$ of the Stokeslet with λ_1 fixed at 0.6. We see that the plot for $c=3$ remains below the $q_\theta=0$ line and hence the flow is counterclockwise on the surface of the cylinder.

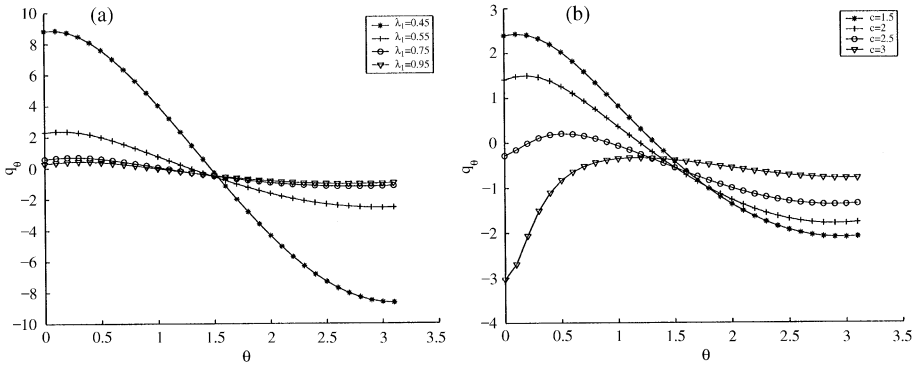

Fig. 14. Fluid velocity on the surface of a cylinder of radius $a=4$ due to a Stokeslet with its axis along y-direction located at $(r=c,\ \theta=0)$: (a) effect of slip with fixed $c=2.0$; (b) effect of different Stokeslet location for a fixed $\lambda_1=0.6$.

5. Conclusion

We have demonstrated here the effect of slip on steady flows inside an infinitely long cylinder induced by three types of line singularities: rotlet, source, and Stokeslets with their axes either along x- or y-direction. In each of these cases, an exact solution for the stream function has been derived in closed form which have been subsequently used to plot streamline topologies for these flows. These shed light on the qualitative features of the flows such as eddies and stagnation points, etc. In all cases, eddies of different sizes and shapes are found to occur. The flow topologies in the case of a pair of equal rotlets are found to be qualitatively similar to vortex mixing flows. The streamline plots illustrate the existence of interior saddle points (hyperbolic points) in these flows. The hyperbolic points depend on both slip as well as the location of the singularities. One might expect that the flow induced by a pair of rotlets considered here could exhibit chaos under a given time-periodic perturbation. This in turn could make the stirring more efficient for the cases in which the unperturbed flow possesses a hyperbolic fixed point.

In the source–sink flow discussed above, both the slip parameter and the locations of the primary singularities have significant effects on the flow patterns. The cores of the eddies in these flows move closer to the source or the cylinder wall depending on whether the primary source and sink are located at equidistance from the origin or otherwise. The existence of secondary vortices in source–sink flows in the absence of inertia does not seem to have been noticed in the literature. This flow model might be used in certain processes involving simultaneous suction and injection of a fluid. Eddies also appear in Stokeslet induced flows and the flow patterns here depend on the slip parameter and the locations of the Stokeslets. Finally, analytical results and the streamline topologies presented here may inspire one to design new experiments on mixing or chaos, and also to use these for validating numerical simulations on such flows in bounded domains.

Acknowledgements

This research has been partially supported by the interdisciplinary research program of the Office of the Vice President for Research and Associate Provost for Graduate Studies under grant IRI-98 and IRI-99.

References

[1] B.Y. Ballal, R.S. Rivlin, Flow of a Newtonian fluid between eccentric rotating cylinders: inertial effects, Arch. Rational Mech. Anal. 62 (1976) 237–294.
[2] S.C. Jana, G. Metcalfe, J.M. Ottino, Experimental and computational studies of mixing in complex Stokes flows: the vortex mixing flow and multicellular cavity flows, J. Fluid Mech. 269 (1994) 199–246.
[3] K.B. Ranger, Eddies in two-dimensional Stokes flow, Int. J. Eng. Sci. 18 (1980) 181–190.
[4] V.V. Meleshko, H. Aref, A blinking rotlet model for chaotic advection, Phys. Fluids A 8 (1996) 3215–3217.
[5] Lord Rayleigh, On the flow of a viscous liquids, especially in two dimensions, Philos. Mag. 5 (1893) 354–372.
[6] H. Aref, Stirring by chaotic advection, J. Fluid Mech. 143 (1984) 1–24.
[7] A.J. Lichtenberg, M.A. Lieberman, Regular and Stochastic Motion, Springer, New York, 1983.
[8] J. Chaiken, R. Chevray, M. Tabor, Q.M. Tan, Experimental study of Lagrangian turbulence in a Stokes flow, Proc. Ry. Soc. London. Ser. A 408 (1986) 165–174.
[9] H. Aref, S. Balachander, Chaotic advection in a Stokes flow, Phys. Fluids 29 (1986) 3515–3521.
[10] P.D. Swanson, J.M. Ottino, A comparative computational and experimental study of chaotic mixing of viscous fluids, J. Fluid Mech. 213 (1990) 227–249.
[11] A.B. Basset, A Treatise on Hydrodynamics, Vol. 2, Deighton, Bell and Co., Cambridge, 1888.
[12] B.U. Felderhof, Force density on a sphere in linear hydrodynamics. I. Fixed sphere, stick boundary conditions, Physica A 84 (1976a) 557–568.
[13] B.U. Felderhof, Force density on a sphere in linear hydrodynamics. I. Moving sphere, mixed boundary conditions, Physica A 84 (1976b) 569–576.
[14] R. Schmitz, B.U. Felderhof, Creeping flow about a sphere, Physica A 136 (1982) 77–98.
[15] B.U. Felderhof, R.B. Jones, Hydrodynamics scattering theory of flow about a sphere, Physica A 136 (1986) 77–98.
[16] S.A. Wymer, A. Lakhtakia, R.S. Engel, Extinction cross-section of an arbitrary body in a viscous incompressible fluid, Phys. Rev. E 52 (1995) 1857–1865.
[17] S.A. Wymer, A. Lakhtakia, R.S. Engel, The Huygens principle for flow around an arbitrary body in a viscous incompressible fluid, Fluid Dyn. Res. 17 (1996) 212–223.